A Hybrid Model of 2d-DCT and 2d-Mycielski Algorithm for Hourly Global Solar Irradiation

Mehmet FİDAN[1], Mine SERTSÖZ[1], Mehmet KURBAN[2]
[1]*Eskişehir Technical University Voc. School of Transportation 26140, Eskisehir, Turkey*
[2]*Bilecik Seyh Edebali University Elec. and Elec. Eng. Dept. 11210, Bilecik, Turkey*
mfidan@eskisehir.edu.tr

***Abstract*—In this work, hourly solar irradiation is defined as a two-dimensional discrete signal. This two-dimensional discrete signal is modeled by a novel hybrid approach, which includes both deterministic and stochastic processes. The variables of the two-dimensional model are the hour and the day of each solar irradiation measurement. The deterministic process is modeled by two-dimensional discrete cosine transform. The two-dimensional discrete cosine transform finds the coefficients of two-dimensional cosine harmonics of the solar irradiation data. In the proposed model, two-dimensional discrete cosine transform is applied at two levels for obtaining an accurate deterministic model. The stochastic process is modeled by two-dimensional Mycielski algorithm, which is developed for searching repeats of two-dimensional neighborhood pattern of the sample to be predicted in the data and making predictions which depend on the closest repeat of the largest neighborhood pattern. A novel model is obtained for hourly solar irradiation, which fits both deterministic and stochastic processes by the combination of two models. The proposed model is benchmarked with the selected distinguished methods in the literature. The obtained comparative results demonstrate success of the proposed model.**

***Index Terms*—discrete cosine transform, forecasting, modeling, prediction, solar energy.**

I. INTRODUCTION

Solar energy sources have capability to supply an important proportion of the energy demand. The forecast of the solar energy potential in any location is a crucial problem for projection and management of large solar projects. The energy efficiency can be satisfied with a successful solar irradiation forecasting. The solar irradiation forecasting can be applied for short-term and long-term with respect to purpose. In addition, medium-term solar irradiation forecasting can also be applied. Nowcasting comprises the detailed description of the current weather along with forecasts obtained by extrapolation for a period of 0-6 h ahead [1].

In the literature, solar irradiation is classified as a stochastic process according to its unpredictable harmonics. Nevertheless, some deterministic models are also proposed in literature. Nemes and Munteanu use clear sky global irradiance model on Shuttle Radar Topography Mission (SRTM) database [2]. Nemes and Munteanu develop a daily solar irradiation model by considering the effect of sun's zenith angle and atmospheric transmittance in their research. Their model defines the daily solar irradiation by the summation of a constant, a sine harmonic and a cosine harmonic. In another recent research, Rezaie-Balf et al. construct a multivariate adaptive regression spline method (MARS) based on complete empirical mode decomposition with adaptive noise (CEEMDAN) as a daily solar radiation predictor [3]. Kaplanis obtains a hourly solar radiation model with a summation of constant and a single cosine harmonic [4]. Kaplanis and Kaplani also improve the model of Kaplanis by handling dependency of amplitude of the cosine harmonic on sun zenith's angle and sun's declination angle [5]. Kaplani and Kaplanis finally improve a stochastic simulation model for PV system by the consideration of hourly solar radiation model [6].

For a hybrid deterministic-stochastic model of hourly solar irradiation, a Fourier series and NN is used in a previous research, where the Fourier series approach gives the sinusoidal harmonics of the solar irradiation [7]. Moghaddam and Seifi use 2D-FIR filters for hourly prediction of wind speed [8]. Moghaddam and Seifi also develop a FIR-NN hybrid model for prediction renewable sources on smart grids [9]. A. Anvari-Moghaddam, H. Monsef, A. Rahimi-Kian, and H. Nance finally improve a 2D-FIR model for hourly solar radiation forecasting [10].

The artificial neural network (ANN) is one of the choices in the broad solar forecasting literature [11-17]. ANN techniques for estimating irradiation have been shown to have greater accuracy than other techniques such as linear, nonlinear and fuzzy approaches by Yadav and Chandel [11]. L. Benali, G. Notton, A. Fouilloy, C. Voyant, and R. Dizene propose a hybrid model of ANN and random forest method for solar radiation forecasting in a recent research [18]. A model based on combining of k-means clustering method and the ANN was also proposed by Benmouiza and Cheknane [19]. S. Ghimire, R. C. Deo, N. Raj, and J. Mi applied convolutional neural network (CNN) with long short-term memory network as a solar radiation predictor [20]. A hybrid method of exponential smoothing state space (ESSS) model and artificial neural network (ANN) for solar radiation forecasting was proposed by Z. Dong, D. Yang, T. Reindl and W. M. Walsh [21].

A solar radiation estimation method, which uses a combination of the satellite images, solar radiation data and a variety of other atmospheric and weather satellite data to generate solar radiation maps to study the sun and its behavior at different geographical coordinates (latitude and longitude) was presented by Polo et al. [22].

A hybrid machine learning (ML) method by combining support vector regression (SVR), gradient boosted regression (GBR) and random forest regression (RFR), which was called as European Center for Medium range Weather Forecasting (ECMWF) model, was proposed by Y. Gala, Á. Fernández, J. Díaz, and J. R. Dorronsoro [23]. In

Digital Object Identifier 10.4316/AECE.2020.02006

other research, a hybrid method of SOM, support vector regression (SVR) and particle swarm optimization (PSO) was applied for hourly solar radiation forecasting [24]. A novel method named as SVM–FFA is developed by hybridizing the Support Vector Machines (SVMs) with Firefly Algorithm (FFA) to predict the monthly mean horizontal global solar radiation using three meteorological parameters of sunshine duration, maximum temperature and minimum temperature as inputs [25]. A Kernel SVM method with structural variable selection (KSVM-SVS) was proposed and applied to the four real-world case studies in China by Jiang and Dong [26].

Eight regression-based models for estimating hourly diffuse solar irradiation at the ground level were proposed by Paulescu and Blaga [27]. Three empirical sunshine based models are compared correlating the monthly mean daily global solar radiation on a horizontal surface with monthly mean sunshine records for Nigde, Turkey by Gungor et al. [28]. The particle swarm optimization method was also mentioned for the applications on the solar photovoltaics in the review study of Khare and Rangnekar [29]. A hybrid model of random forests and FFA for prediction of the hourly global solar irradiation for a location in Malaysia was constructed by Ibrahim and Khatib [30]. A sparse quadratic radial basis function neural network (QRBF) is applied to determine relevant meteorological variables to forecast the global horizontal irradiance [31] A novel clustering model based on TB K-means algorithm as a forecasting method was developed by Azimi, Ghayekhloo and Ghofrani [32].

Global Solar Radiation on Horizontal Surface (GSRHS), was developed to estimate the average hourly global solar radiation on the horizontal surfaces was proposed by Pandey and Soupir [33]. The estimations of GSRHS have strong correlation with the exact measurements of solar irradiation. A global solar radiation model for the data on Osmaniye in Turkey was applied by Yaniktepe, Kara and Ozalp [34].

A model, which is a novel adaptive approach, which includes linear prediction filter and clearness index-based decision maker was proposed by Akarslan and Hocaoglu [35]. The authors also developed a novel short-term prediction methodology, which considers the past records of data to predict solar irradiance value for the desired hours by Akarslan and Hocaoglu [36]. To predict next hour's solar irradiance data, a day similar to the prediction day is searched in the history. A model based on using the one-dimensional Mycielski and Markov hybrid model, which achieves better accuracy results than the single one-dimensional Mycielski model was developed by Hocaoglu and Serttas [37].

In this study, hourly solar radiation data are taken as a single two-dimensional discrete signal depending to hour and day. There are two main reasons to work in two dimensions. First one is to investigate frequencies of harmonics depend on not only the hour variable, but also the day variable. Second one is to investigate the two-dimensional patterns in the data, which are constructed from sequential samples on hour and day axis in two-dimensional discrete representation. This two-dimensional signal is taken as a summation of deterministic and stochastic processes. The proposed model is applied on two-year hourly solar irradiation data of Ankara city, which belong to 2015 and 2016 years. First year data (2015) are used for construction of 2D-DCT model and second year data are used for test of the model. Ankara irradiation data are shown in Figure 1.

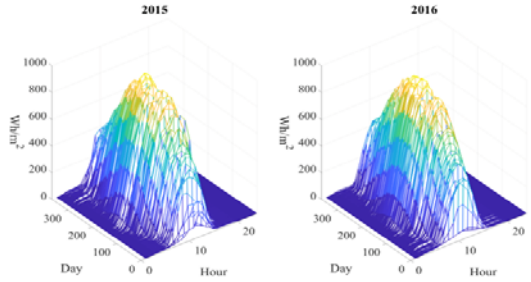

Figure 1. Solar Irradiation Data of Ankara for 2015 and 2016

For the comparison of the method's performance with other region with similar seasonal characteristics, the proposed hybrid method is also applied on three-year hourly solar irradiation data of Izmir, which belong to 2003, 2004 and 2005 years. For that data 2D-DCT model is constructed from the data of year 2003 and the hybrid model is tested on the data of both 2004 and 2005 years. Izmir irradiation data are shown in Figure 2.

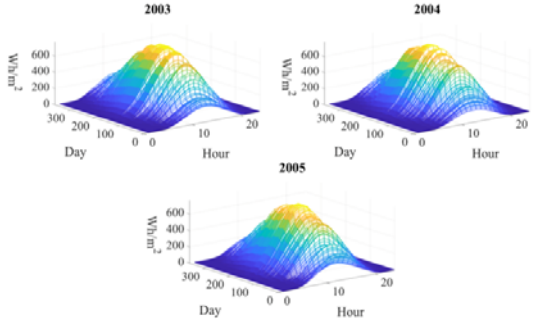

Figure 2. Solar Irradiation Data of Izmir for 2003, 2004 and 2005

In the proposed 2D-DCT-Mycielski hybrid model, the deterministic process is modeled by two-dimensional discrete cosine transform because of even symmetry and cosine-like behavior of the signal [38, 39]. The accuracy of the 2D-DCT model is improved by applying it at two-level. The decision of the necessary number of the 2D-DCT model is given by the minimization of the mean absolute percentage error (MAPE) of 2D-DCT model at the first level, which is detailly explained in Section II.

The stochastic component is modeled by two-dimensional Mycielski algorithm, which is based on searching random repeats of the two-dimensional patterns [40]. The 2D-Mycielski algorithm is derived by 1D-Mycielski Algorithm [41]. In the literature, 1D-Mycielski Algorithm was used for wind speed prediction [42] and synthetic wind speed data generation [43]. For the efficient utilization of the 2D-Mycielski algorithm, a scanning routine is chosen which depends on Manhattan metric [44]. Moreover, a tolerated distance is defined instead of Hamming distance for detect repetitions of real-valued 2D-patterns [40, 45]. The detailed explanation of 2D-Mycielski algorithm is given in Section-III.

The hybridization of 2D-DCT and 2D-Mycielski algorithm is explained in Section IV. The performance of the method is compared with Mycielski-Markov model [37], GSRHS model [33] and a similarity-based prediction model [36] via RRMSE, MAPE, R and R2 metrics in Section V

and finally a detailed analysis of the comparative results is done in Section VI as a conclusion.

II. Two-Dimensional Discrete Cosine Transform

Discrete Cosine Transform is a Fourier based transform, which explains signals in terms of cosine harmonics, was firstly proposed by Ahmed et al. [46]. This transform is mostly used in Jpeg based image compression and MP3 based audio compression [39]. According to the even-symmetry of cosine function, it fits even symmetric signals. The general description of original discrete cosine transform has four forms. The most used form of one dimensional DCT is DCT-II can be explained as in (1) and (2).

$$y[k]=\sqrt{\frac{2}{N}}\sum_{n=1}^{N}x[n]\frac{1}{\sqrt{1+\delta_{k1}}}\varphi(k,n) \tag{1}$$

The coefficient δ_{k1} is Kronecker delta, which is 1 if k is equal to 1 and 0 otherwise. This coefficient is necessary for normalization of the projections of DCT-II.

$$\varphi(k,n)=\cos\left(\frac{\pi}{2N}(2n-1)(k-1)\right) \tag{2}$$

$\varphi(k,n)$ is the function, which is used to calculate projections of the $x[n]$ discrete signal on the cosine functions with different frequencies.

If the number of time parameters is increased to 2 from 1, the 2D-DCT can be expressed as (3), (4) and (5).

$$y[k_1,k_2]=\alpha_{k_1}\alpha_{k_2}\sum_{n_1=1}^{N_1}\sum_{n_2=1}^{N_2}x[n_1,n_2]\varphi_1(k_1,n_1)\varphi_2(k_2,n_2) \tag{3}$$

$$\alpha_{k_i}=\begin{cases}\dfrac{1}{\sqrt{N_i}}, & k_i=1\\ \sqrt{\dfrac{2}{N_i}}, & N_i\geq k_i>1\end{cases}, \quad \text{where } i=1 \text{ or } 2 \tag{4}$$

Instead of $\sqrt{2/[N(1+\delta_{k1})]}$ in DCT-II, 2D-DCT uses multiplication of α_{k_1} and α_{k_2} coefficients, because of the necessity of an additional normalization coefficient for additional dimension. The effect of Kronecker delta on the coefficients are defined in terms of a condition which depends on whether if k_i is 1 or not. The value 1 of k_i corresponds first cosine harmonic with the lowest frequency.

$$\varphi_i(k_i,n_i)=\cos\left(\frac{\pi(2n_i+1)k_i}{2N_i}\right), \quad \text{where} \quad i=1 \text{ or } 2 \tag{5}$$

$\varphi_1(k_1,n_1)$ and $\varphi_2(k_2,n_2)$ are the function, which are used to calculate projections of the $x[n_1,n_2]$ 2D-discrete signal on the cosine functions of first dimension and second dimension correspondingly with different frequencies.

The 2D-DCT model makes its predictions by inverse transform of the 2D-DCT (2D-IDCT) which can be generalized as (6).

$$\hat{x}[n_1,n_2]=\sum_{k_1=1}^{N_1}\sum_{k_2=1}^{N_2}\alpha_{k_1}\alpha_{k_2}y[k_1,k_2]\varphi_1(k_1,n_1)\varphi_2(k_2,n_2) \tag{6}$$

In this study, the proposed 2D-DCT model includes two levels of 2D-DCT. First level models of the strong harmonics of the irradiation data. Second level models detailed harmonics of the irradiation data. The proposed 2D-DCT model for modeling deterministic process in solar irradiation is illustrated as block diagram in Figure 3.

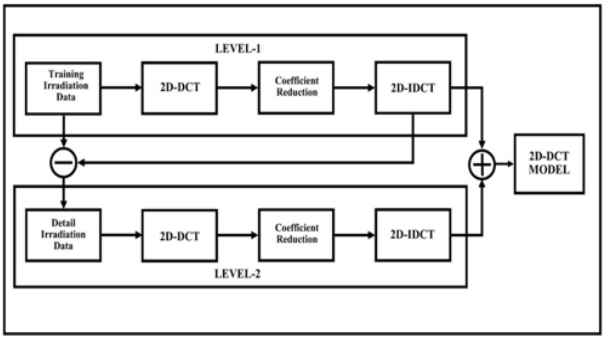

Figure 3. 2D-DCT Model for Solar Irradiation

Hourly data for one-year period include 365x24 number of samples. Consequently 2D-DCT transformation of the data generates 365x24 number of coefficients. Equations (3)-(5) can be modified for solar irradiation data as in (7)-(11).

$$y_{L1}[k_1,k_2]=\alpha_{k_1}\alpha_{k_2}\sum_{d=1}^{365}\sum_{h=1}^{24}I_{Train}[d,h]\varphi_1(k_1,d)\varphi_2(k_2,h) \tag{7}$$

$y_{L1}[k_1,k_2]$ is the special form of (3) which is used for first level of 2D-DCT, where N_1 is taken as 365 for dimension of day and N_2 is taken as 24 for dimension of hour.

$$\alpha_{k_1}=\begin{cases}\dfrac{1}{\sqrt{365}}, & k_1=1\\ \sqrt{\dfrac{2}{365}}, & k_1>1\end{cases} \tag{8}$$

$$\alpha_{k_2}=\begin{cases}\dfrac{1}{\sqrt{24}}, & k_1=1\\ \sqrt{\dfrac{1}{12}}, & k_1>1\end{cases} \tag{9}$$

Similarly, the coefficients expressed in (8) and (9) are the special forms of (4) used for the normalization in dimension of day and dimension of hour correspondingly.

$$\varphi_1(k_1,d)=\cos\left(\frac{\pi(2d+1)k_1}{730}\right) \tag{10}$$

$$\varphi_2(k_2,h)=\cos\left(\frac{\pi(2h+1)k_2}{48}\right) \tag{11}$$

The projection functions expressed in (10) and (11) are derived from (5), where $2N_i$ is equal to 730 for the dimension of day and 48 for the dimension of hour.

Equation (6) can be modified as (12) for the solar irradiation predictions of first level of 2D-DCT model.

$$\hat{I}_{L1}[d,h]=\sum_{k_1=1}^{D}\sum_{k_2=1}^{H}\alpha_{k_1}\alpha_{k_2}y_{L1}[k_1,k_2]\varphi_1(k_1,d)\varphi_2(k_2,h) \tag{12}$$

In (7)-(12), "*I*" denotes solar irradiation, "*d*" denotes day variable and "*h*" denotes hour variable. "*D*" is equal to 365 and "*H*" is equal to 24, if all $y_{L1}[k_1,k_2]$ coefficients are used for 2D-IDCT. However, it is not necessary to use all

$y_{L1}[k_1,k_2]$ coefficients as the number of coefficients can be reduced according to satisfaction of minimum absolute percentage error (MAPE).

$$\text{MAPE}\left(I_{Train},\hat{I}_{L1}\right)=\frac{100\%}{365\times 24}\sum_{d=1}^{365}\sum_{h=1}^{24}\left|\frac{\varepsilon_{L1}[d,h]}{I_{Train}[d,h]}\right| \quad (13)$$

MAPE for all possible (*D*, *H*) combinations for Level-1 2D-DCT model are shown as Figure 4.

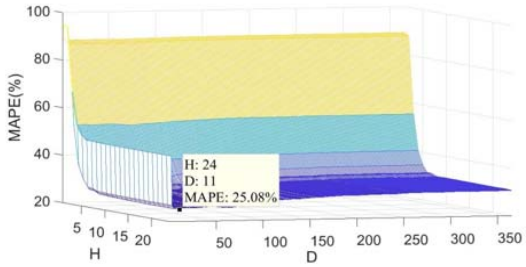

Figure 4. MAPE of Level-1 2D-DCT Model

The prediction error of Level-1 2D-DCT model is defined by (14).

$$\varepsilon_{L1}[d,h]=I_{Train}[d,h]-\hat{I}_{L1}[d,h] \quad (14)$$

The selection criteria for the optimum (*D, H*) couple is given in (15).

$$(D_{opt},H_{opt})=\arg\min_{(D,H)}\left[\text{MAPE}\left(I_{Train},\hat{I}_{L1}\right)\right] \quad (15)$$

According to (15), D_{opt} is found as 11 and H_{opt} is found as 24. Thus 2D-DCT model can be expressed by 11x24=264 coefficients instead of 365x24=8760 coefficients. As a result, 2D-DCT model is reduced 3% of the full model.

In Level-2, the 2D-DCT coefficients of the prediction error of Level-1 is computed by (16).

$$y_e[k_1,k_2]=\alpha_{k_1}\alpha_{k_2}\sum_{d=1}^{365}\sum_{h=1}^{24}\varepsilon_{L1}[d,h]\varphi_1(k_1,n_1)\varphi_2(k_2,n_2) \quad (16)$$

The reduction rate for the number of 2D-DCT coefficients in Level-1 is also applied to the Level-2 2D-DCT part. The error of Level-1 is predicted by the inverse 2D-DCT of reduced number of 2D-DCT coefficients as shown in (17).

$$\hat{I}_e[d,h]=\sum_{k_1=1}^{11}\sum_{k_2=1}^{24}\alpha_{k_1}\alpha_{k_2}y_e[k_1,k_2]\varphi_1(k_1,n_1)\varphi_2(k_2,n_2) \quad (17)$$

The complete model is represented also by 264 coefficients as seen in (18).

$$\hat{I}_{L2}[d,h]=\hat{I}_{L1}[d,h]+\hat{I}_e[d,h] \quad (18)$$

Calculated values for the Level-1 and Level-2 2D-DCT coefficients can be seen in Figure 5 for Ankara and Figure 6 for Izmir.

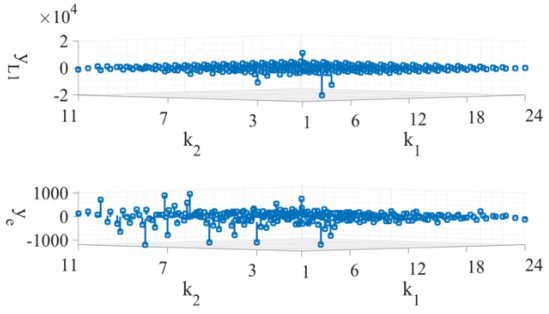

Figure 5. $y[k_1,k_2]$ of Level-1 and Level-2 2D-DCT for Ankara

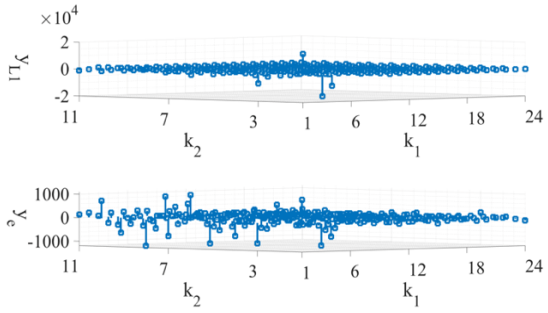

Figure 6. $y[k_1,k_2]$ of Level-1 and Level-2 2D-DCT for Izmir

If the presented $y_{L1}[k_1,k_2]$ coefficients in Figure-5 and Figure-6 are investigated, it can be seen that strongest harmonics are found in three location for both Izmir and Ankara data, where (k_1,k_2) positions are equal to (1,1), (1,3) and (3,1). The coefficient of the harmonic represented in location (1,1) is in positive direction and the other two are in negative direction. This is the most critical information found by Level-1 2D-DCT.

If the presented $y_e[k_1,k_2]$ coefficients in Figure-5 and Figure-6 are investigated, it can be seen that the location of the coefficients for the strongest harmonics are not unique for Izmir and Ankara data, because these coefficients belong detail harmonics which are changing location by location. On the other hand, these detail coefficients are flactuating in the exponential-like decreasing boundaries, where the coefficients are converging zero, while the frequencies of their corresponding harmonics converge to infinity. Based on these findings, it can be concluded that Level-2 2D-DCT is necessary to extract information about solar radiation detail harmonics.

The solar irradiation prediction of one level and two level 2D-DCT model can be seen in Figure 7 for Ankara and Figure 8 for Izmir. As seen in the figures, the shape of the prediction data obtained with the contribution of Level-2 2D-DCT coefficients resembles the shape of the actual data more than the Level-1 2D-DCT predictions.

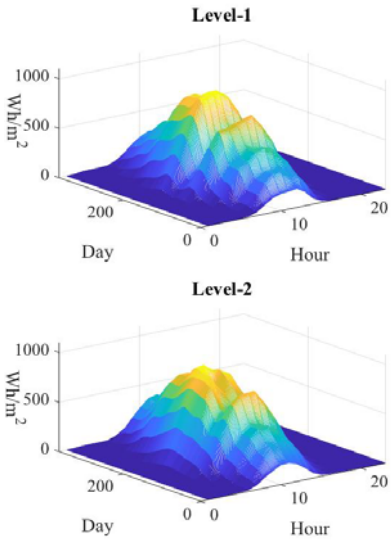

Figure 7. Predictions of Level-1 and Level-2 2D-DCT Model for Ankara

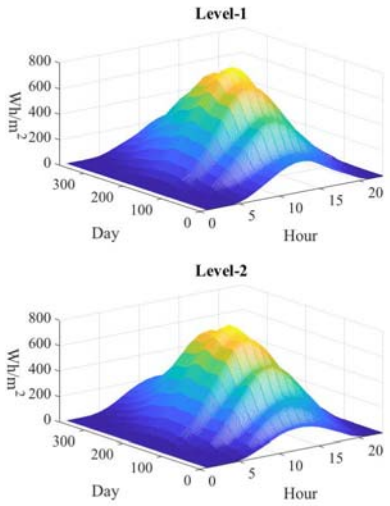

Figure 8. Predictions of Level-1 and Level-2 2D-DCT Model for Izmir

III. Two-Dimensional Mycielski Algorithm

2D-Mycielski algorithm is a search-based prediction algorithm, which makes its prediction by finding the largest repetition of 2D-neighborhood pattern of the sample to be predicted in the infinite history [40]. This algorithm is derived from the 1D-Mycielski algorithm [41-43], which can be expressed by equations (19)-(23). The definition of the infinite history is given by (19).

$$x_{History}\left(n_1+1\right)=x\left[0:n_1\right] \tag{19}$$

The black-box definition of the 1D-Mycielski is given in (20) which depends on the infinite history given in (19).

$$\hat{x}\left[n+1\right]=f_{\text{1D-MYC}}\left(x_{History}\left(n_1+1\right)\right) \tag{20}$$

The original algorithm searches the neighborhood pattern of the sample to be predicted which is defined as (21).

$$x_{NBHD}\left(i,L\right)=x\left[\left(i-L\right):\left(i-1\right)\right] \tag{21}$$

Algorithm will stop to search the neighborhood pattern, if it finds the largest pattern expressed in (22).

$$p=\underset{i}{\text{argmax}}\, L\left\{i\left|x_{NBHD}\left(i,L\right)=x_{NBHD}\left(n+1,L\right)\right.\right\} \tag{22}$$

where $L<i<\left(n-L+1\right)$.

The sample in the infinite history, which is pointed by the location found in (22), is taken as the prediction value of 1D-Mycielski algorithm as shown in (23).

$$f_{\text{1D-MYC}}\left(x\left[1:n\right]\right)=x\left[p\right] \tag{23}$$

For 2D-Mycielski algorithm can be generalized as equations (24)-(28), by the two-dimensional modification of equations (19)-(23).

The definition of the infinite history can be expanded as in (24) for 2D-discrete space.

$$x_{History}\left(n_1+1,n_2+1\right)=\begin{bmatrix}x\left[0:n_1,0:n_2+1\right]\\ x\left[n_1+1,0:n_2\right]\end{bmatrix} \tag{24}$$

The black-box definition of the 2D-Mycielski algorithm can be shown as in (25).

$$\hat{x}\left[n_1+1,n_2+1\right]=f_{\text{2D-MYC}}\left(x_{History}\left(n_1+1,n_2+1\right)\right) \tag{25}$$

The neighborhood pattern of any sample with an L-by-L size, where the sample itself is excluded, can be expressed by (26).

$$x_{NBHD}\left(i,j,L\right)=\begin{bmatrix}x\left[\left(i-L\right):\left(i-1\right),\left(j-L\right):j\right]\\ x\left[i,\left(j-L\right):\left(j-1\right)\right]\end{bmatrix} \tag{26}$$

The closest and the largest repetition for the neighborhood pattern of the sample to be predicted is located at the position given in (27).

$$\left(p,q\right)=\arg\max_{(i,j)} L\left\{\left(i,j\right)\left|\begin{matrix}x_{NBHD}\left(i,j,L\right)\\ =\\ x_{NBHD}\left(n_1+1,n_2+1,L\right)\end{matrix}\right.\right\} \tag{27}$$

where $L<i<\left(n_1-L+1\right)$ and $L<j<\left(n_2-L+1\right)$.

The sample in the infinite history, which is pointed by the location found in (27), is taken as the prediction value of 2D-Mycielski algorithm as shown in (28).

$$f_{\text{2D-MYC}}\left(x_{History}\left(n_1+1,n_2+1\right)\right)=x\left[p,q\right] \tag{28}$$

In 2D-Mycielski algorithm, there are two important problems for determination of neighborhood pattern. First problem is the shape of the searched pattern. Second problem is widening routine of the searched pattern at each iteration. The applied shape and widening routine are shown for 2D-Mycielski in Figure 9.

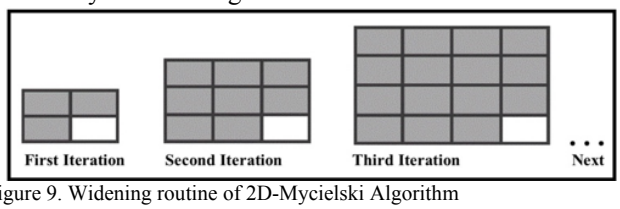

Figure 9. Widening routine of 2D-Mycielski Algorithm

Infinite history is the region of the 2D-data for scanning the previous repetition of the searched pattern. The limits of the infinite history are identified by the index values of the sample to be predicted, which stands left upper side of the sample to be predicted. The neighborhood pattern must be excluded from the scanned region to avoid the intersection of searched pattern and probable previous repetition.

The prediction value is the sample at the right lower corner of the found largest previous repetition with respect to (27). In the case of multiple repetitions for the largest searched pattern, the closest one should be taken as default repeat. Therefore, scanning routine should be from closer region to farther region of the infinite history.

Closeness of the regions is identified by d_1 metric, which are also called as Manhattan metric as in (29) [44].

$$d_1\left(x,y\right)=\left|x_1-y_1\right|+\left|x_2-y_2\right| \tag{29}$$

The infinite history defined in (24) and the scanning routine of the infinite history for finding the closest repetition of the searched pattern via (29) for a single step of 2D-Mycielski are illustrated in Figure 10. The chosen scanning routine depends on the Manhattan metric.

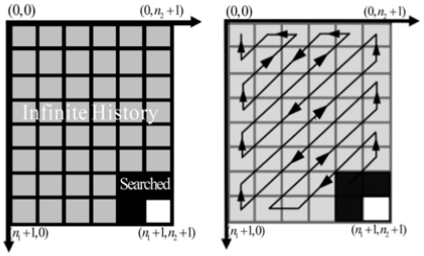

Figure 10. Infinite history and scanning routine of 2D-Mycielski

Comparison of neighborhood pattern and the candidate for the repetition is applied by a similarity test. In the binary Mycielski Algorithm, Hamming distance is used as similarity test [45]. Hamming distance of two binary valued vectors is calculated by (30).

$$d_{\text{Hamming}} = (v_1, v_2) = \sum_{i=1}^{n} \left[v_1[i] \oplus v_2[i] \right] \quad (30)$$

Hamming distance must be zero to accept two patterns as alike. Otherwise, they are assumed different. In the real valued series, similarity test will fail to catch similar patterns with Hamming distance, since the repetition of a real value is improbable. The tolerated distance, which is used instead of Hamming distance is expressed by (31) and (32) for achieving the real value problems.

$$f_{\text{tolerated}}(x_1, x_2) = \begin{cases} 0, |x_1 - x_2| < \dfrac{\max\{|x_1|, |x_2|\}}{10} \\ 1, |x_1 - x_2| \geq \dfrac{\max\{|x_1|, |x_2|\}}{10} \end{cases} \quad (31)$$

The tolerated distance between two compared samples is defined by the function in (31). If the output of the $f_{tolarated}(x_1, x_2)$ are 0, x_1 and x_2 are considered as alike and otherwise they are considered as different.

$$d_{\text{tolerated}}(M_1, M_2) = \sum_i \sum_j f_{\text{tolerated}}(M_1[i,j], M_2[i,j]) \quad (32)$$

The distance between two compared patterns are defined by the summation of distances between their corresponding samples as shown in (32), where each distance between sample couples is defined by (31).

As in Hamming distance, if and only if the tolerated distance is 0, then the compared patterns will be assumed as alike.

The final improvement of 2D-Mycielski algorithm is about the default prediction that will be used whereas the smallest searched pattern is not found in the history. If the smallest searched pattern is not repeated in the infinite history, the prediction value will be taken as zero in the original Mycielski algorithm. On the other hand, the proposed 2D-Mycielski algorithm takes the default prediction as the mean of neighbor values $x[n_1, n_2+1]$ and $x[n_1+1, n_2]$ instead of zero for unrepeated neighborhoods.

IV. Proposed Hybrid Model

2D-DCT model is a deterministic approach, which gives same predictions for the single (d,h) moment of all years. However, solar irradiation has also a stochastic component, which shows different behavior for each year. In the hybrid model, the prediction error of the Level-2 2D-DCT Model for 2016 solar irradiation data is predicted by proposed 2D-Mycielski algorithm. The summation of prediction for the error of 2D-DCT and the prediction of the 2D-DCT model give the ultimate prediction for hourly solar irradiation. This hybrid model is represented by a block diagram shown in Figure 11 and expressed by (33)-(35).

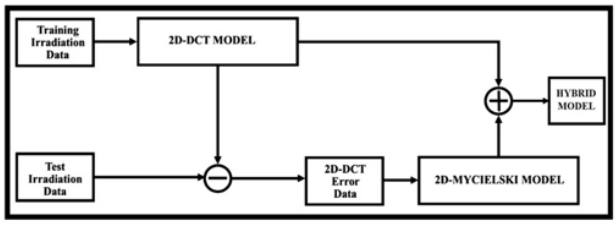

Figure 11. Structure of Proposed Deterministic-Stochastic Hybrid Model

$$\varepsilon_{L2}[d,h] = I_{Test}[d,h] - \hat{I}_{L2}[d,h] \quad (33)$$

In (33), $\varepsilon_{L2}[d,h]$ denotes the error between Level-2 2D-DCT predictions and the last years exact measurement data.

$$\hat{\varepsilon}_{L2}[d,h] = f_{\text{2D-MYC}}(\varepsilon_{L2,History}(d,h)) \quad (34)$$

In (34), $\hat{\varepsilon}_{L2}[d,h]$ denotes prediction of 2D-Mycielski for the error of Level-2 2D-DCT found in (33).

$$\hat{I}_{Hybrid}[d,h] = \hat{I}_{L2}[d,h] + \hat{\varepsilon}_{L2}[d,h] \quad (35)$$

The comparative prediction errors of Level-1 2D-DCT, Level-2 2D-DCT and the hybrid model can be shown as Figure 12 for Ankara.

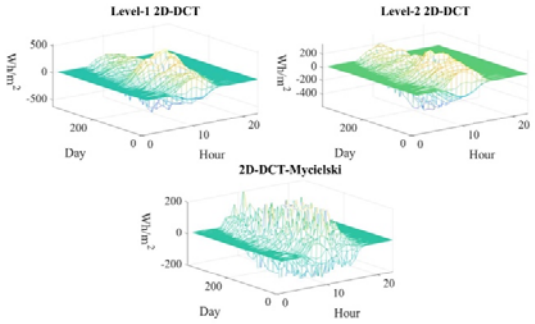

Figure 12. Prediction errors of Level-1 2D-DCT, Level-2 2D-DCT and 2D-DCT-Mycielski for Ankara (2016)

In Figures 13-15 predictions of the Level-1 2D-DCT, Level-2 2D-DCT and proposed hybrid model are plotted with respect to exact measurements for Ankara correspondingly.

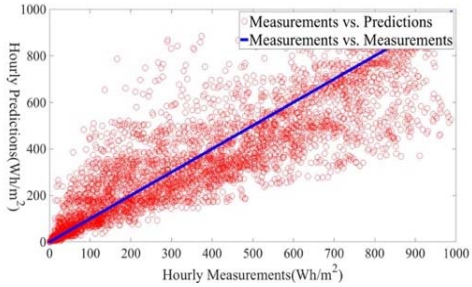

Figure 13. Exact Measurements vs. Predictions of Level-1 2D-DCT for Ankara (2016)

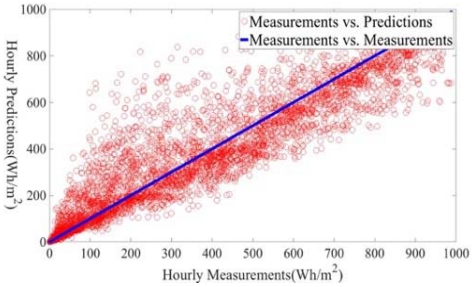

Figure 14. Exact Measurements vs. Predictions of Level-2 2D-DCT for Ankara (2016)

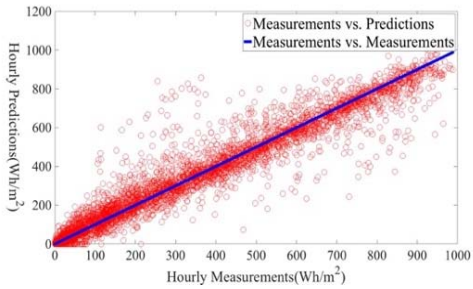

Figure 15. Exact Measurements vs. Predictions of 2D-DCT-Mycielski for Ankara (2016)

The ultimate predictions of the proposed hybrid model are illustrated in Figure 16 for Ankara (2016).

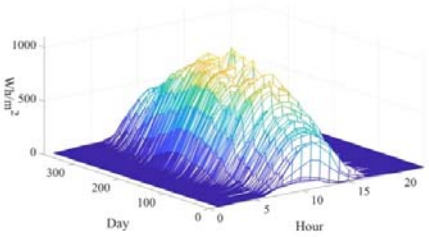

Figure 16. Prediction of 2D-DCT-Mycielski Model for Ankara (2016)

The comparative prediction errors of Level-1 2D-DCT, Level-2 2D-DCT and the hybrid model can be shown as Figure 17 for Izmir.

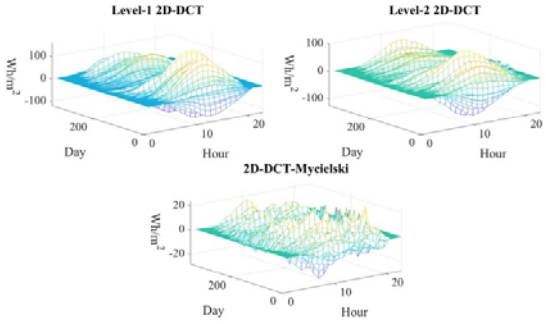

Figure 17. Prediction errors of Level-1 2D-DCT, Level-2 2D-DCT and 2D-DCT-Mycielski for Izmir (2005)

Measurements vs. Predictions are also illustrated in Figures18-20 for Izmir.

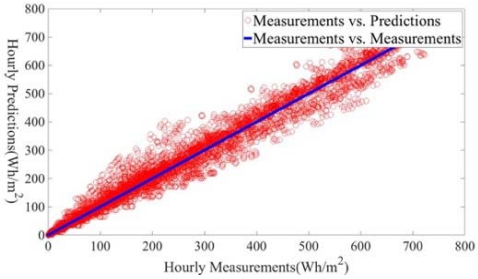

Figure 18. Exact Measurements vs. Predictions of Level-1 2D-DCT for Izmir (2005)

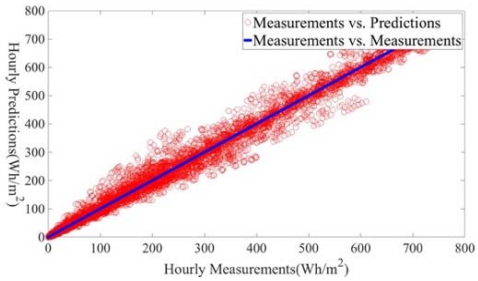

Figure 19. Exact Measurements vs. Predictions of Level-2 2D-DCT for Izmir (2005)

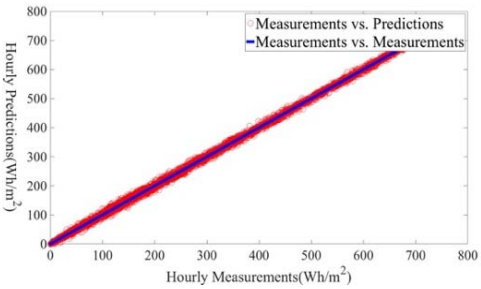

Figure 20. Measurements vs. Predictions of 2D-DCT-Mycielski for Izmir (2005)

Figure 14 and Figure 19 show the improvement of Level-2 2D-DCT on Level-1 2D-DCT for both Ankara and Izmir regions. Similarly, Figure 15 and Figure 20 show the improvement of proposed hybrid 2D-DCT-Mycielski model on Level-2 2D-DCT. Figure 12 and Figure 17 also demonstrate this improvement of the 2D-Mycielski algorithm in Figure-15 and Figure-20. Thus, while instant errors of the Level-2 2D-DCT model overflowed the (-200, +200) kW/m^2 band, instant errors of the Hybrid model remained in the (-200, +200) kW/m^2 band for Ankara. Similarly, while instant errors of the Level-2 2D-DCT model reached the (-100, +100) kW/m^2 band, instant errors of the Hybrid model remained in the (-20, + 20) kW/m^2 band for Izmir. As a result of the fact that 2D-Mycielski algorithm strengthens the model by capturing random components that the 2D-DCT model cannot capture, the numerical results also prove the necessity of hybridizing with 2D-Mycielski algorithm for a sensitive prediction.

The ultimate predictions of the proposed hybrid model are illustrated in Figure 21 for Izmir (2005).

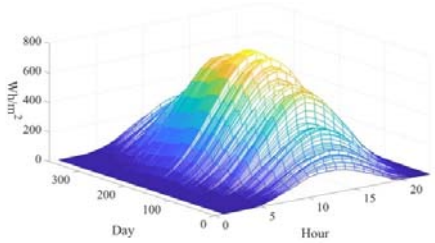

Figure 21. Prediction of 2D-DCT-Mycielski Model for Izmir (2005)

In Figure 22 and Figure 23, the predictions of the proposed hybrid model and exact measured values are shown in one-dimensional time-domain representation for Ankara and Izmir correspondingly.

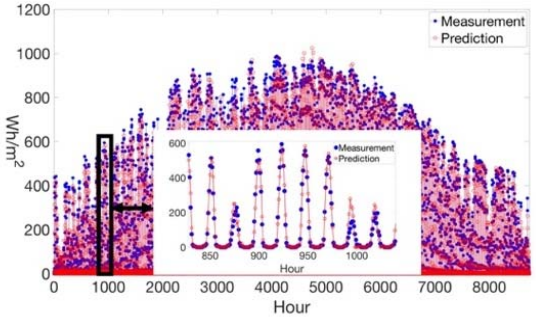

Figure 22. Pred. of 2D-DCT-Mycielski Model and Exact Measurements for Ankara (2016)

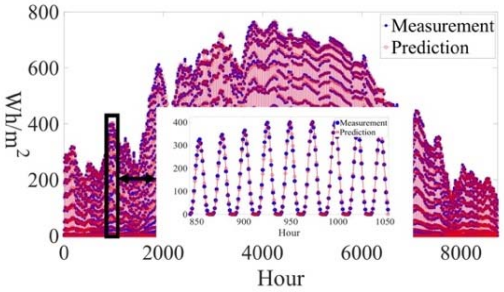

Figure 23. Pred. of 2D-DCT-Mycielski Model and Exact Measurements for İzmir (2005)

Table I indicates the statistical characteristics RMS and mean (μ) of the measurement data of hourly solar irradiation of Ankara for the years 2015 and 2016, Izmir for the years 2003, 2004 and 2005, and prediction data of Level-1 2D-DCT model, Level-2 DCT model and mixed 2D-DCT-Mycielski model for both Ankara and Izmir regions.

TABLE I. RMS AND MEAN OF MEASUREMENT AND PREDICTION DATA

	RMS	μ
Measurement (Ankara-2015)	304.7902	173.1018
Measurement (Ankara-2016)	319.5962	184.1625
Level-1 2D-DCT (Ankara)	292.9279	173.1018
Level-2 2D-DCT (Ankara)	318.4575	184.1625
2D-DCT-Myc(Ankara)	319.1048	184.1933
Measurement (Izmir-2003)	294.1736	205.8584
Measurement (Izmir-2004)	298.5565	210.6404
Measurement (Izmir-2005)	289.1044	202.0251
Level-1 2D-DCT (Izmir)	292.1522	202.4979
Level-2 2D-DCT (Izmir)	288.0733	202.0612
2D-DCT-Myc (Izmir-2004)	298.1598	207.2203
2D-DCT-Myc (Izmir-2005)	288.8038	198.9632

Table II indicates the statistical characteristics standard deviation (σ) and variance (σ^2) of the same data used in Table I.

TABLE II. STANDARD DEVIATION AND VARIANCE OF MEASUREMENT AND PREDICTION DATA

	σ	σ^2
Measurement (Ankara-2015)	250.8785	62940
Measurement (Ankara-2016)	261.2158	68234
Level-1 2D-DCT (Ankara)	236.3236	55849
Level-2 2D-DCT (Ankara)	259.8211	67507
2D-DCT-Myc(Ankara)	260.5925	67908
Measurement (Izmir-2003)	210.1559	42162
Measurement (Izmir-2004)	211.5932	44772
Measurement (Izmir-2005)	206.8142	42772
Level-1 2D-DCT (Izmir)	210.6006	44353
Level-2 2D-DCT (Izmir)	205.3348	42162
2D-DCT-Myc (Izmir-2004)	214.3929	45964
2D-DCT-Myc (Izmir-2005)	209.3473	43826

V. COMPARATIVE RESULTS

The performance of the predictors can be measured via several metrics. Two key achievements are measured in the performance measurements of the predictors. The first one is how well the predictor minimizes the prediction error, and the other is how strongly the generated predictions have a correlation with the actual data.

The two of the most objective metrics for the error measurement can be listed as relative root mean square error (rRMSE %) and mean absolute percentage error (MAPE %). rRMSE % and MAPE %, which do not depend on the RMS or amplitude of the measurement data, because their definitions include normalization. Therefore, the error of different models can be compared with the rRMSE% and MAPE% metrics, even though they were not applied on the same region.

The detailed definitions of rRMSE %, MAPE %, are given in (36) and (37).

$$\text{rRMSE\%} = \frac{\sqrt{\frac{1}{365\cdot 24}\sum_{d=1}^{365}\sum_{h=1}^{24}\left[\varepsilon(d,h)\right]^2}}{\frac{1}{365\cdot 24}\sum_{d=1}^{365}\sum_{h=1}^{24}\left[I(d,h)\right]}\cdot 100\% \tag{36}$$

$$\text{MAPE\%} = \frac{100\%}{365\times 24}\sum_{d=1}^{365}\sum_{h=1}^{24}\left|\frac{\varepsilon(d,h)}{I(d,h)}\right| \tag{37}$$

The comparative rRMSE and MAPE performances of Level-1 2D-DCT model, Level-2 2D-DCT model, the proposed hybrid 2D-DCT-Mycielski model and the chosen similar studies in the literature are given in Table III.

TABLE III. COMPARATIVE ERRORS OF PROPOSED MODELS

	rRMSE %	MAPE%
Level-1 2D-DCT (Ankara-2016)	51.2445	32.5373
Level-1 2D-DCT (Izmir-2004)	15.3063	22.4112
Level-1 2D-DCT (Izmir-2005)	16.3169	24.6453
Level-2 2D-DCT (Ankara-2016)	14.6367	6.8761
Level-2 2D-DCT (Izmir-2004)	9.2828	5.7959
Level-2 2D-DCT (Izmir-2005)	12.3309	7.2778
2D-DCT-Myc (Ankara-2016)	10.5662	4.9633
2D-DCT-Myc (Izmir-2004)	7.8215	2.9593
2D-DCT-Myc (Izmir-2005)	7.4627	3.0872
Myc-Markov (Afyon)	39.4	13
Myc-Markov (Antalya)	36.3	10.7554
GSRHS (Albuquerque)	28	16
Sim. Based (Afyon)	24.1407	14.7709

The correlation between predictions and actual data can be measured by the coefficients R and R^2, which give strong information about goodness of the fit of the proposed model on the measurement data. The coefficient R denotes the Pearson correlation coefficient and the coefficient R^2 denotes the coefficient of determination.

The comparative R and R^2 performances of Level-1 2D-DCT model, Level-2 2D-DCT model, the proposed hybrid 2D-DCT-Mycielski model and the chosen similar studies in the literature are given in Table IV.

TABLE IV. COMPARATIVE CORRELATIONS OF PROPOSED MODELS

	R	R^2
Level-1 2D-DCT (Ankara-2016)	0.9339	0.8695
Level-1 2D-DCT (Izmir-2004)	0.9891	0.9768
Level-1 2D-DCT (Izmir-2005)	0.9877	0.9746
Level-2 2D-DCT (Ankara-2016)	0.9947	0.9894
Level-2 2D-DCT (Izmir-2004)	0.9957	0.9915

Level-2 2D-DCT (Izmir-2005)	0.9927	0.9855
2D-DCT-Myc (Ankara-2016)	0.9972	0.9945
2D-DCT-Myc (Izmir-2004)	0.9972	0.9939
2D-DCT-Myc (Izmir-2005)	0.9976	0.9947
Myc-Markov (Afyon)	0.8511	0.8506
Myc-Markov (Antalya)	0.8479	0.8320
GSRHS (Albuquerque)	0.98	0.99
Sim. Based (Afyon)	0.9572	NA*

*Not Available

The detailed explanations of correlation coefficients R and R^2 are given in (38) and (39) correspondingly.

$$R = \frac{\sum_{d=1}^{365}\sum_{h=1}^{24}\left[I_0(d,h)\cdot\hat{I}_0(d,h)\right]}{\sqrt{\sum_{d=1}^{365}\sum_{h=1}^{24}\left[I_0(d,h)\right]^2}\cdot\sqrt{\sum_{d=1}^{365}\sum_{h=1}^{24}\left[\hat{I}_0(d,h)\right]^2}} \quad (38)$$

$$R^2 = 1 - \frac{\sum_{d=1}^{365}\sum_{h=1}^{24}\left[\varepsilon(d,h)\right]^2}{\sum_{d=1}^{365}\sum_{h=1}^{24}\left[I_0(d,h)\right]^2} \quad (39)$$

In (36), (37) and (39), $\varepsilon(d,h)$ denotes the instant prediction error, which can be expressed by (40).

$$\varepsilon(d,h) = I(d,h) - \hat{I}(d,h) \quad (40)$$

In (38) and (39), $I_0(d,h)$ denotes the zero mean solar irradiation measurement data, which can be expressed by (41).

$$I_0(d,h) = I(d,h) - \mathrm{E}[I] \quad (41)$$

In (38) and (39), $\hat{I}_0(d,h)$ denotes the zero mean solar irradiation prediction data, which can be expressed by (42).

$$\hat{I}_0(d,h) = \hat{I}(d,h) - \mathrm{E}\left[\hat{I}\right] \quad (42)$$

VI. Conclusion

In this study, a three layered hourly solar radiation model was developed. The first two layer are Level-1 2D-DCT, Level-2 2D-DCT, which are used to determine deterministic part of the solar irradiation. The last layer is the 2D-Mycielski, which is used to model stochastic process of the solar irradiation. Each layer of the model can be used as a separate predictor. However, each new layer makes it possible to make more accurate predictions than the previous layer as seen in Table III and Table IV.

Figure 5 and Figure 6, which show 2D-DCT coefficients found in Level-1 and Level-2, give an idea about the fundamental harmonics of the solar irradiation data. In addition, these coefficients achieve to approximate the overall solar radiation data with a smaller number of coefficients. In the proposed model, 264 coefficients are used in Level-1 2D-DCT and 264 coefficients are used in Level-2 2D-DCT for approximation of 8760 hourly samples. That means the number of data required was reduced to 6% of the initial number of data.

The main reason of choosing 2D-Mycielski algorithm as the predictor of stochastic component is its capability to catch 2D repeated patterns in the data, which cannot be achieved by 1D-Mycielski algorithm. The contribution of the 2D-Mycielski algorithm is also proved by the performance results listed in Table III and Table IV. rRMSE is reduced to below 11% and MAPE is reduced to below 5% by the 2D-Mycielski based improvement. The predictions of the hybrid 2D-DCT-Mycielski method show strongest correlation with exact measurements in terms of R and R^2 compared to similar methods in the literature.

In concern with other methods in the literature which are not included to the comparative results, firstly it should be emphasized that the proposed method provides a short-term(hourly) prediction, which is not offered by Digital Elevation Model [2] or CEEMDAN Decomposition-Based MARS Model[3]. In addition, it does not need the sun zenith's angle and sun's declination angle as in methods of Kaplanis method [5]. Moreover, the proposed model makes not only a prediction of the solar irradiation, but also gives strong information about the frequencies of the fundamental and detailed harmonics of the solar irradiation data by the contribution of 2D-DCT model, which can not be obtained by regression, FIR filters, SVM, ANN or CNN based methods [8-33]. Finally, the proposed method includes a novelty about hybridizing with 2D-Mycielski algorithm which relies on repetition of the 2D patterns in the history of the error data of the 2D-DCT model, which compose stochastic component of the solar irradiation. This 2D-largest pattern search based prediction method has not been applied in the literature, whose positive contribution was proved by the comparative results.

In future studies, 2D-DCT-Mycielski method can be improved by algorithmic optimizations on 2D-Mycielski algorithm to reduce the prediction error. Moreover, 2D-DCT algorithm can be hybridized with different stochastic models. Finally, 2D-DCT algorithm can also be hybridized with most common machine learning and deep learning methods as ANN, SVM, CNN or improved versions of these methods.

Acknowledgment

The authors acknowledge to the General Directorate of Meteorology, Forestry and Water Affairs Ministry of the republic of Turkey for the supply of Solar Irradiation Hourly data.

References

[1] https://www.wmo.int/pages/prog/amp/pwsp/Nowcasting.htm

[2] C. Nemes and F. Munteanu, "Potential Solar Irradiance Assessment based on a Digital Elevation Model," Advances in Electrical and Computer Engineering, vol. 11, no. 4, pp. 89-92, 2011. doi:10.4316/AECE.2011.04014

[3] M. Rezaie-Balf et al., "Forecasting Daily Solar Radiation Using CEEMDAN Decomposition-Based MARS Model Trained by Crow Search Algorithm," Energies, vol. 12, no. 8, 2019. doi:10.3390/en12081416

[4] S. N. Kaplanis, "New methodologies to estimate the hourly global solar radiation; Comparisons with existing models," (in English), Renewable Energy, vol. 31, no. 6, pp. 781-790, May 2006. doi:10.1016/j.renene.2005.04.011

[5] S. Kaplanis and E. Kaplani, "A model to predict expected mean and stochastic hourly global solar radiation I(h;nj) values," Renewable Energy, vol. 32, no. 8, pp. 1414-1425, 2007. doi:10.1016/j.renene.2006.06.014

[6] E. Kaplani and S. Kaplanis, "A stochastic simulation model for reliable PV system sizing providing for solar radiation fluctuations," (in English), Applied Energy, vol. 97, pp. 970-981, Sep 2012. doi:10.1016/j.apenergy.2011.12.016

[7] M. Fidan, Ö.N. Gerek and F.O. Hocaoğlu, "Harmonic analysis based hourly solar radiation forecasting model," IET Renewable Power Generation, vol. 9, no. 3, pp. 218-227, 2015. doi:10.1049/iet-rpg.2014.0057

[8] A. A. Moghaddam and A. R. Seifi, "An advanced strategy for wind speed forecasting using expert 2-D FIR filters," Advances in Electrical and Computer Engineering, vol. 10, no. 4, pp. 103-110, 2010. doi:10.4316/aece.2010.04017

[9] A. A. Moghaddam and A. R. Seifi, "Study of forecasting renewable energies in smart grids using linear predictive filters and neural networks," (in English), Iet Renewable Power Generation, vol. 5, no. 6, pp. 470-480, Nov 2011. doi:10.1049/iet-rpg.2010.0104

[10] A. Anvari-Moghaddam, H. Monsef, A. Rahimi-Kian, and H. Nance, "Feasibility study of a novel methodology for solar radiation prediction on an hourly time scale: A case study in Plymouth, United Kingdom," Journal of Renewable and Sustainable Energy, vol. 6, no. 3, 2014. doi:10.1063/1.4878847

[11] A. K. Yadav and S. S. Chandel, "Solar radiation prediction using Artificial Neural Network techniques: A review," Renewable and Sustainable Energy Reviews, vol. 33, pp. 772-781, 2014. doi:10.1016/j.rser.2013.08.055

[12] M. H. Al-Shamisi, A. H. Assi, and H. A. N. Hejase, "Artificial Neural Networks for Predicting Global Solar Radiation in Al Ain City - Uae," International Journal of Green Energy, vol. 10, no. 5, pp. 443-456, 2013. doi:10.1080/15435075.2011.641187

[13] A. Mellit, S. Sağlam, and S. A. Kalogirou, "Artificial neural network-based model for estimating the produced power of a photovoltaic module," Renewable Energy, vol. 60, pp. 71-78, 2013. doi:10.1016/j.renene.2013.04.011

[14] S. Quesada-Ruiz, A. Linares-Rodríguez, J. A. Ruiz-Arias, D. Pozo-Vázquez, and J. Tovar-Pescador, "An advanced ANN-based method to estimate hourly solar radiation from multi-spectral MSG imagery," Solar Energy, vol. 115, pp. 494-504, 2015. doi:10.1016/j.solener.2015.03.014

[15] C. Voyant, P. Randimbivololona, M. L. Nivet, C. Paoli, and M. Muselli, "Twenty four hours ahead global irradiation forecasting using multi-layer perceptron," Meteorological Applications, vol. 21, no. 3, pp. 644-655, 2014. doi:10.1002/met.1387

[16] N. Zhang and P. K. Behera, "Solar radiation prediction based on recurrent neural networks trained by Levenberg-Marquardt backpropagation learning algorithm," presented at the 2012 IEEE PES Innovative Smart Grid Technologies (ISGT), 2012. doi:10.1109/ISGT.2012.6175757

[17] G. Notton, C. Voyant, A. Fouilloy, J. L. Duchaud, and M. L. Nivet, "Some Applications of ANN to Solar Radiation Estimation and Forecasting for Energy Applications," Applied Sciences, vol. 9, no. 1, 2019. doi:10.3390/app9010209

[18] L. Benali, G. Notton, A. Fouilloy, C. Voyant, and R. Dizene, "Solar radiation forecasting using artificial neural network and random forest methods: Application to normal beam, horizontal diffuse and global components," Renewable Energy, vol. 132, pp. 871-884, 2019. doi:10.1016/j.renene.2018.08.044

[19] K. Benmouiza and A. Cheknane, "Forecasting hourly global solar radiation using hybrid k-means and nonlinear autoregressive neural network models," Energy Conversion and Management, vol. 75, pp. 561-569, 2013. doi:10.1016/j.enconman.2013.07.003

[20] S. Ghimire, R. C. Deo, N. Raj, and J. Mi, "Deep solar radiation forecasting with convolutional neural network and long short-term memory network algorithms," Applied Energy, vol. 253, 2019. doi:10.1016/j.apenergy.2019.113541

[21] Z. Dong, D. Yang, T. Reindl, and W. M. Walsh, "Satellite image analysis and a hybrid ESSS/ANN model to forecast solar irradiance in the tropics," Energy Conversion and Management, vol. 79, pp. 66-73, 2014. doi:10.1016/j.enconman.2013.11.043

[22] J. Polo et al., "Solar resources and power potential mapping in Vietnam using satellite-derived and GIS-based information," Energy Conversion and Management, vol. 98, pp. 348-358, 2015. doi:10.1016/j.enconman.2015.04.016

[23] Y. Gala, Á. Fernández, J. Díaz, and J. R. Dorronsoro, "Hybrid machine learning forecasting of solar radiation values," Neurocomputing, vol. 176, pp. 48-59, 2016. doi:10.1016/j.neucom.2015.02.078

[24] Z. Dong, D. Yang, T. Reindl, and W. M. Walsh, "A novel hybrid approach based on self-organizing maps, support vector regression and particle swarm optimization to forecast solar irradiance," Energy, vol. 82, pp. 570-577, 2015. doi:10.1016/j.energy.2015.01.066

[25] L. Olatomiwa, S. Mekhilef, S. Shamshirband, K. Mohammadi, D. Petković, and C. Sudheer, "A support vector machine-firefly algorithm-based model for global solar radiation prediction," Solar Energy, vol. 115, pp. 632-644, 2015. doi:10.1016/j.solener.2015.03.015

[26] H. Jiang and Y. Dong, "Forecast of hourly global horizontal irradiance based on structured Kernel Support Vector Machine: A case study of Tibet area in China," Energy Conversion and Management, vol. 142, pp. 307-321, 2017. doi:10.1016/j.enconman.2017.03.054

[27] E. Paulescu and R. Blaga, "Regression models for hourly diffuse solar radiation," Solar Energy, vol. 125, pp. 111-124, 2016. doi:10.1016/j.solener.2015.11.044

[28] A. Gungor, M. Gokcek, F. Yalcin, A. Kocer, I. F. Yaka, and G. T. Sardogan, "Determining the best model for estimation the monthly mean daily global solar radiation on a horizontal surface - A case study in Nigde, Turkey," World Journal of Engineering, vol. 12, no. 3, pp. 307-312, 2015. doi:10.1260/1708-5284.12.3.307

[29] A. Khare and S. Rangnekar, "A review of particle swarm optimization and its applications in Solar Photovoltaic system," Applied Soft Computing, vol. 13, no. 5, pp. 2997-3006, 2013. doi:10.1016/j.asoc.2012.11.033

[30] I. A. Ibrahim and T. Khatib, "A novel hybrid model for hourly global solar radiation prediction using random forests technique and firefly algorithm," Energy Conversion and Management, vol. 138, pp. 413-425, 2017. doi:10.1016/j.enconman.2017.02.006

[31] H. Jiang, "A novel approach for forecasting global horizontal irradiance based on sparse quadratic RBF neural network," Energy Conversion and Management, vol. 152, pp. 266-280, 2017. doi:10.1016/j.enconman.2017.09.043

[32] R. Azimi, M. Ghayekhloo, and M. Ghofrani, "A hybrid method based on a new clustering technique and multilayer perceptron neural networks for hourly solar radiation forecasting," Energy Conversion and Management, vol. 118, pp. 331-344, 2016. doi:10.1016/j.enconman.2016.04.009

[33] P. K. Pandey and M. L. Soupir, "A new method to estimate average hourly global solar radiation on the horizontal surface," Atmospheric Research, vol. 114-115, pp. 83-90, 2012. doi:10.1016/j.atmosres.2012.05.012

[34] B. Yaniktepe, O. Kara, and C. Ozalp, "The global solar radiation estimation and analysis of solar energy: Case study for Osmaniye, Turkey," International Journal of Green Energy, vol. 14, no. 9, pp. 765-773, 2017. doi:10.1080/15435075.2017.1329148

[35] E. Akarslan and F. O. Hocaoglu, "A novel adaptive approach for hourly solar radiation forecasting," Renewable Energy, vol. 87, pp. 628-633, 2016. doi:10.1016/j.renene.2015.10.063

[36] E. Akarslan and F. O. Hocaoglu, "A novel method based on similarity for hourly solar irradiance forecasting," (in English), Renewable Energy, vol. 112, pp. 337-346, Nov 2017. doi:10.1016/j.renene.2017.05.058

[37] F. O. Hocaoglu and F. Serttas, "A novel hybrid (Mycielski-Markov) model for hourly solar radiation forecasting," Renewable Energy, vol. 108, pp. 635-643, 2017. doi:10.1016/j.renene.2016.08.058

[38] A. K. Jain, "5.6 The Cosine Transform," in Fundamentals of Digital Image ProcessingEnglewood Cliffs, NJ: Prentice Hall, 1989, pp. 150-153.

[39] W. B. Pennebaker and J. L. Mitchell, JPEG still image data compression standard. Van Nostrand Reinhold, 1993.

[40] M. Fidan and Ö. N. Gerek, "Mycielski Based 2d-Predictive Image Coding Algorithm," Applied Mechanics and Materials, vol. 850, pp. 144-151, 2016. doi:10.4028/www.scientific.net/AMM.850.144

[41] P. Jacquet, W. Szpankowski, and I. Apostol, "A universal predictor based on pattern matching," (in English), Ieee Transactions on Information Theory, vol. 48, no. 6, pp. 1462-1472, Jun 2002. doi:10.1109/TIT.2002.1003834

[42] F. O. Hocaoğlu, M. Fidan, and Ö. N. Gerek, "Mycielski approach for wind speed prediction," Energy Conversion and Management, vol. 50, no. 6, pp. 1436-1443, 2009. doi:10.1016/j.enconman.2009.03.003

[43] M. Fidan, F. O. Hocaoglu, and O. N. Gerek, "Improved synthetic wind speed generation using modified Mycielski approach," (in English), International Journal of Energy Research, vol. 36, no. 13, pp. 1226-1237, Oct 2012. doi:10.1002/er.1893

[44] P. E. Black. (12-25-2019). Manhattan Distance. Available: https://www.nist.gov/dads/HTML/manhattanDistance.html

[45] G. Forney Jr, "Generalized minimum distance decoding," Information Theory, IEEE Transactions on, vol. 12, no. 2, pp. 125-131, 1966. doi:10.1109/TIT.1966.1053873

[46] N. Ahmed, T. Natarajan, and K. R. Rao, "Discrete Cosine Transform," IEEE Transactions on Computers, vol. C-23, no. 1, pp. 90-93, 1974. doi:10.1109/T-C.1974.223784